ACS Catalysis

Letter

pubs.acs.org/acscatalysis

Tuning Enzyme Kinetics through Designed Intermolecular Interactions Far from the Active Site

Yingning Gao,[†] Christopher C. Roberts,[‡] Jie Zhu,[§] Jyun-Liang Lin,[†] Chia-en A. Chang,[‡] and Ian Wheeldon*,[†]

[†]The Department of Chemical and Environmental Engineering, University of California, Riverside, Riverside, California 92521, United States

[‡]The Department of Chemistry, University of California, Riverside, Riverside, California 92521, United States

[§]The Department of Biochemistry, University of California, Riverside, Riverside, California 92521, United States

Supporting Information

ABSTRACT: Enzyme−DNA nanostructures were designed to introduce new substrate−enzyme interactions into their reactions, which altered enzyme kinetics in a predictable manner. The designed enzymes demonstrate a new strategy of enzyme engineering based on the rational design of intermolecular interactions outside of the active site that enhance and control enzyme kinetics. Binding interactions between tetramethylbenzidine and DNA attached to horseradish peroxidase (HRP) resulted in a reduced Michaelis constant (K_M) for the substrate. The enhancement increased with stronger interactions in the micromolar range, resulting in a 2.6 fold increase in k_{cat}/K_M. The inhibition effect of 4-nitrobenzoic hydrazide on HRP was also significantly enhanced by tuning the binding to HRP−DNA. Lastly, binding of a nicotinamide adenine dinucleotide (NAD(H)) cofactor mimic, nicotinamide mononucleotide (NMN(H)), to an aldo-keto reductase (AdhD) was enhanced by introducing NMN(H)−DNA interactions.

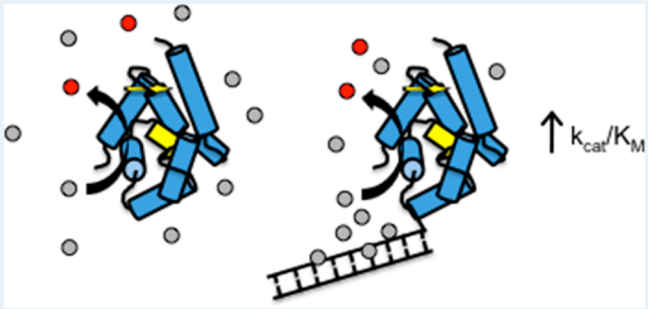

KEYWORDS: *biocatalysis, biophysics, enzymes, nanostructures, protein design*

Evolved interactions between substrates and noncatalytic residues drive high catalytic rates that are essential to the biological function of many enzymes. Charged amino acids on the surface of superoxide dismutase create an electrostatic field that directs the enzyme's substrate to the active site.[1,2] These intermolecular interactions drive catalysis to rates upward of 5×10^9 M^{-1} s^{-1}.[3,4] Acetylcholinesterase terminates synaptic transmissions by hydrolyzing acetylcholine at an active site buried within an enzymatic cleft.[5] Electrostatic and pi stacking interactions between substrates and residues at the top of the cleft facilitate catalysis, producing diffusion-limited rates.[6,7] From a catalysis perspective, these two examples suggest a new strategy for enzyme engineering—the rational design of intermolecular interactions outside of an enzyme's active site that enhance and control enzyme kinetics.

Traditional approaches to enzyme engineering are well-known:[8−11] rational design of active sites can increase selectivity and rate; directed evolution can create activity toward new substrates, and improve activity, selectivity, and stability; and immobilization can be used to maintain high activity over time and in harsh conditions. Some of the successful outcomes from these approaches may result in new, beneficial substrate−enzyme interactions, but it is not necessarily their intent. Here, we engineer enzyme kinetics by introducing and tuning intermolecular interactions between enzyme substrates and modified enzymes. The hypothesis is that the effective molarity of a substrate can be increased by introducing beneficial interactions between an enzyme and its substrate. The increase in effective molarity is expected to result in a decrease in the apparent binding constant and a corresponding increase in catalytic efficiency (k_{cat}/K_M), or in the case of an inhibitor, enhanced inhibition effect.

The hypothesis was tested with two different enzymes, an aldo-keto reductase (AdhD) and horseradish peroxidase (HRP), and three reactions. Substrate−enzyme interactions were introduced by modifying each enzyme with short double stranded (ds) DNA. The strands were 20 base pair (bp) sequences with quantified binding interactions to the substrates of interest including the following: nicotinamide mononucleotide (NMN(H)), a mimic to nicotinamide adenine dinucleotide (NAD(H)) and cofactor to the oxidation reaction of AdhD;[12] tetramethylbenzidine (TMB), an immunoassay reagent for HRP;[13−15] and 4-nitrobenzoic hydrazide (4-NBH), an inhibitor to HRP.[16]

Received: November 5, 2014
Published: February 24, 2015

DOI: 10.1021/acscatal.5b00130
ACS Catal. 2015, 5, 2149−2153

The first example was the oxidation of TMB with HRP. Our previous work identified micromolar binding affinity of TMB to DNA.[17] With this as a starting point, we used AutoDock simulation software[18] to identify the possibility of sequence-dependent binding. Simulations with a 50-member library of randomly generated 10 bp dsDNA sequences predicted weak sequence-dependent binding (Figure S1,S2). From this library, we selected two sequences to characterize experimentally. Assuming 50% GC content, the melting temperature of 10 bp dsDNA is approximately 30 °C, as such the identified 10 bp sequences were repeated to produce DNA1 and DNA2, two 20 bp dsDNA with predicted binding to TMB. A third DNA segment with a scrambled DNA2 sequence was also characterized (Figure 1A). UV−vis titration binding assays of

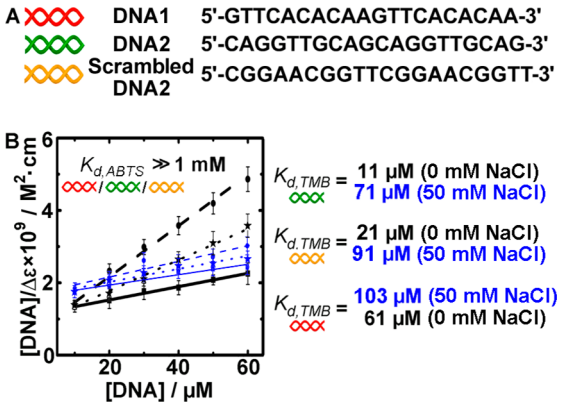

Figure 1. Binding of the HRP substrate TMB with double-stranded DNA. (A) Twenty base pair DNA sequences used in this study. (B) UV−vis binding assays of TMB to DNA, both with and without the addition of 50 mM NaCl.

TMB with DNA1, scrambled DNA2, and DNA2 revealed K_d of 61 ± 6, 21 ± 3, and 11 ± 3 μM, respectively (Figure 1B, Figure S3). Predicted binding poses of TMB on DNA1 and DNA2 suggested binding through short-range interactions (Figure S4), whereas the addition of 50 mM NaCl decreased affinity to both DNA1, scrambled DNA2, and DNA2 (103 ± 12, 92 ± 7, and 80 ± 8 μM, respectively; Figure 1B), suggesting electrostatic interactions were also involved. In comparison to TMB, the common HRP substrate ABTS showed no binding interactions with dsDNA. The reactions of HRP with ABTS and TMB are shown in Figure 2A,B.

Single-stranded (ss) DNA1, DNA-2, and scrambled DNA2 were conjugated to HRP by attaching the amine group of a lysine residue on the surface of HRP to 5′ thiol-modified ssDNA1 and −2. Figure 2C shows the conjugation of DNA1. Gel staining for DNA indicated that HRP was modified and that a complementary strand bound to ssDNA1 to produce HRP(DNA1). Similar results were observed for HRP(DNA2) and HRP(scrambled DNA2) (Figure S5). UV−vis analysis indicated that on average 1 DNA was attached per HRP (Figure S6). The crystal structure of HRP reveals that there are only two lysine residues on the surface of HRP. The close proximity of these residues minimizes potential changes in the observed effects due to the heterogeneity of the HRP(DNA) samples (Figure S7).

Initial rates of HRP, HRP(DNA1), HRP(DNA2), and HRP(scrambled DNA2) with ABTS and TMB substrates are shown in Figure 2D,E. The initial rates of HRP and HRP(DNA) with 300 μM ABTS (a concentration near the K_M for ABTS) and excess H_2O_2 were not statically different (HRP, 221 ± 5 s^{-1}; HRP(DNA1), 224 ± 5 s^{-1}; HRP-(scrambled DNA2), 223 ± 5 s^{-1}; HRP(DNA2), 223 ± 2 s^{-1}). Michaelis−Menten fits to kinetic data of HRP and HRP(DNA) revealed that both k_{cat} and K_M were unaffected by the conjugation of DNA (Figure S8). With 50 μM TMB and excess H_2O_2, the initial rate increased from 18 ± 3 s^{-1} to 30 ± 4 s^{-1} with the addition of DNA1 to HRP. The rate increased to 38 ± 2 s^{-1} with HRP(DNA2) and to 36 ± 2 with HRP(scrambled DNA2). Michaelis−Menten fits to the data (Figure S9) showed that the k_{cat} was unaffected by dsDNA (k_{cat}: HRP, 84 ± 4 s^{-1}; HRP(DNA1), 77 ± 5 s^{-1}; HRP(scrambled DNA2), 79 ± 3 s^{-1}; HRP(DNA2), 81 ± 4 s^{-1}). The TMB−DNA interactions resulted in enhanced binding. The K_M of TMB for unmodified HRP was found to be 60 ± 16 μM (Figure 2F). Apparent K_M ($K_{M,APP}$) decreased to 44 ± 7 μM with a K_d of 103 ± 12 μM (DNA1 with 50 mM NaCl) and decreased to 42 ± 6, 35 ± 6, 28 ± 10, 25 ± 3 and 23 ± 3 μM with increasing interactions between TMB and the

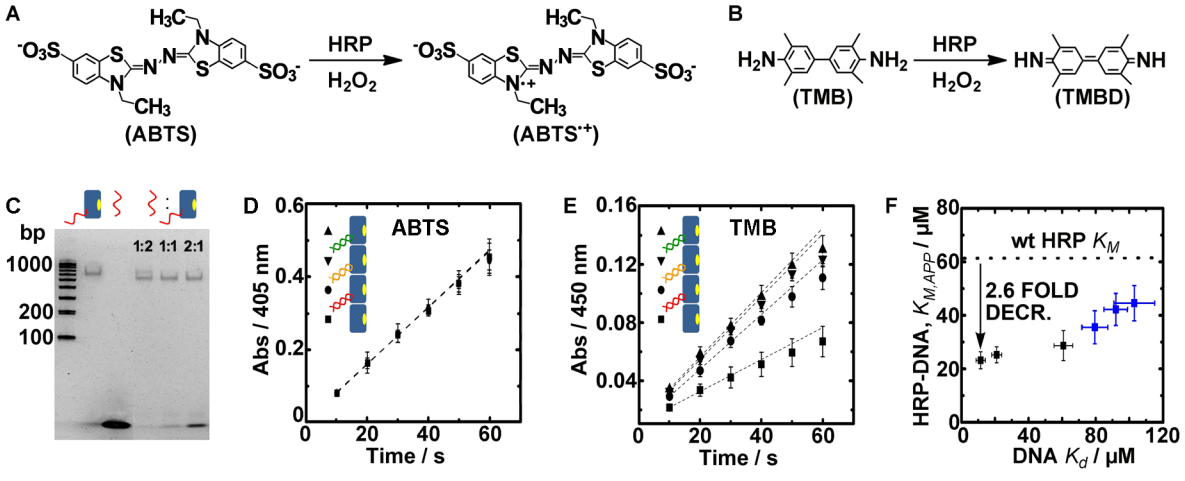

Figure 2. Molecular interactions between substrates and DNA-modified HRP enhance kinetics. (A) HRP reaction with ABTS. (B) HRP reaction with TMB. (C) Electrophoretic mobility shift assay of HRP modified with ssDNA1 and various ratios of a complementary DNA strand. (D,E) Initial rates of HRP and DNA modified HRP with 300 μM ABTS and 50 μM TMB. (F) The observed relationship between $K_{M,APP}$ and K_d of TMB to the DNA conjugated to HRP. Data points shown in blue correspond to binding assays of with 50 mM NaCl shown in Figure 1

DOI: 10.1021/acscatal.5b00130
ACS Catal. 2015, 5, 2149−2153

attached dsDNA (K_d of 92 ± 7, 80 ± 8, 61 ± 6, 21 ± 3 and 11 ± 3 μM, respectively). Conjugation of DNA to HRP was essential to the observed effect as controls with HRP and freely diffusing DNA1 increased $K_{M,APP}$ (Figure S10). Equally critical were the interactions between substrate and enzyme, as the kinetics of HRP with the common substrate ABTS, which showed no binding to DNA1, DNA2, or scrambled DNA2, were unaffected by conjugation with DNA (Figures 2D and S8).

The results presented in Figures 1 and 2 show that the introduction of molecular interactions between substrates and nonactive site structures can enhance HRP kinetics to a limited extent. Due to a decreased $K_{M,APP}$, enzyme efficiency ($k_{cat}/K_{M,APP}$) increased with stronger TMB−HRP(DNA) interactions in the micromolar range, reaching a 2.6 fold increase with a K_d of 11 μM (Figure 2F). It is possible that stronger interactions in nanomolar range could result in additional enhancements, but it is also possible that the effect could be limited to that observed here as stronger interactions may effectively sequester the substrate thus eliminating the effect. The enhancements observed here supports our hypothesis that substrate−enzyme interactions can increase effective molarity. At concentrations below the K_M, increased local concentration of the substrate resulted in increased rate. The effect was minimized at concentrations above the K_M as rate becomes zero order.

The relationship between $K_{M,APP}$ and K_d (Figure 2F) suggests that short-range interactions play a role in the observed effect. Conjugation of DNA to HRP introduces a negative electrostatic field in close proximity to the enzyme that also may contribute to the effect (Figure S11). TMB has neutral charge and a weak electrostatic field, suggesting that a mechanism of increased effective molarity is not long-range electrostatic steering but the electrostatic attractions between DNA1 or DNA2 and TMB when the molecules are in close proximity. Sequence-dependent binding of TMB to DNA suggests that nonelectrostatic interactions are also involved.

The second example was tuning the inhibition of HRP with 4-NBH (Figure 3A). AutoDock simulations predicted that 4-NBH also binds to DNA (Figure S1), as such we characterized 4-NBH binding to DNA1, DNA2, and scrambled DNA2. UV−vis binding assays showed that 4-NBH binds with micromolar affinity to DNA in a sequence-dependent manner (Figure 3B; K_d: scrambled DNA2, 151 ± 9 DNA1, 134 ± 16; DNA2, 69 ± 7 μM). Double reciprocal plots showed classic competitive inhibition trends and nonlinear fits to the data revealed apparent inhibition constants ($K_{I,APP}$) decreasing from 73 ± 5 nM for HRP to 53 ± 5, 42 ± 3 and 36 ± 3 nM for HRP(scrambled DNA2), HRP(DNA1), and HRP(DNA2), respectively (Figure 3C). Again, the effect of altered kinetics increased with increased binding to DNA. Similar to the reaction with TMB, the interactions between 4-NBH and HRP(DNA) supported the hypothesis of increased effective molarity, but in this case causing an increase in inhibition.

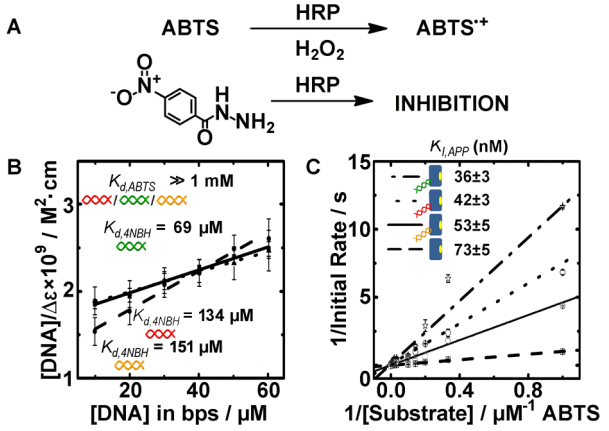

Figure 3. Tuning inhibition of HRP with 4-NBH. (A) Reaction of HRP with ABTS and its inhibition with 4-NBH. (B) UV−vis binding assays of 4-NBH with DNA1, DNA2, and scrambledDNA2. (C) Double reciprocal plots of HRP kinetics with and without DNA modification in the presence of 1 μM of the inhibitor 4-NBH.

The third example of engineering enzyme kinetics through intermolecular interactions focused on AdhD with a NAD(H) mimic (Figure 4A,B). NMN(H) can act as the cofactor to AdhD, and similar to TMB and 4-NBH, it was predicted to bind to dsDNA (Figure S1). DNA1 was predicted to have low micromolar affinity to NMN^+, and therefore, we experimentally characterized binding (Figure 4C; K_d = 3 ± 1 μM) and employed DNA1 to construct AdhD(DNA). No measurable binding was predicted (Figure S1) or observed with NAD(H) (Figure 4C). DNA1 was conjugated to one of a number of free lysines on the outside of the AdhD α/β barrel,[19] and a single free cysteine at the top of the barrel allowed for DNA conjugation near the active site to produce AdhD(DNA1) and AdhD(DNA1)-AS, respectively (Figure 4D, Figure S5).

The kinetics of AdhD with NAD^+ were largely unaffected by the conjugation of DNA(Figure 4E). The ordered bibi rate equation includes a binding term for the cofactor ($K_{D,cof.}$), which can be measured without catalysis.[20,21] Fluorescence binding assays revealed that NAD^+ binding for AdhD with and without DNA was ∼35 μM. Rate (k_{cat}), NAD^+, and diol Michaelis constant ($K_{M,NAD}$, $K_{M,diol}$, respectively) were also unaffected.

NMN^+ cofactor bound less tightly to AdhD than NAD^+, but interactions between NMN^+ and DNA1 resulted in a 1.8-fold decrease in the binding constant of NMN^+ ($K_{D,NMN}$: AdhD, 534 ± 30; AdhD(DNA1), 319 ± 19; AdhD(DNA1)-AS 294 ± 18 μM). NAD(H)-dependent dehydrogenases are known to exhibit substrate inhibition with ordered kinetics, an effect that has been reported for AdhD[12] and was observed here with AdhD(DNA1) and −AS with >10 μM NMN^+. Nonlinear fits to AdhD(DNA1) and -AS kinetics indicated a K_I for NMN^+ of 12 ± 0.7 and 10 ± 0.8 μM, respectively. As expected, when accounting for substrate inhibition k_{cat} of AdhD(DNA1) and -AS where equal to AdhD (k_{cat} ∼ 0.2 s^{-1}; Figure 4E). It is interesting to note that while binding was only enhanced by 1.8-fold the effect on kinetics due to substrate inhibition was greater, with a 4.7-fold decrease in turnover at saturating concentrations of diol and NMN^+ cofactor (Figure S12).

Introducing molecular interactions between NMN^+ and AdhD through conjugation of DNA1 resulted in enhanced cofactor binding, specifically $K_{D,NMN}$. Binding improved slightly when DNA1 was conjugated close to the active site. As was the case with TMB, 4-NBH, HRP(DNA1), and HRP(DNA2), the introduced substrate−enzyme interactions likely resulted in an increase in the effective molarity of the substrate. In this case, the result of increased local concentration was cofactor inhibition and not enhanced catalysis or increased inhibition effect.

Many small molecules bind to DNA with nanomolar to micromolar affinity. Anticancer anthracyclines intercalate base

DOI: 10.1021/acscatal.5b00130
ACS Catal. 2015, 5, 2149−2153

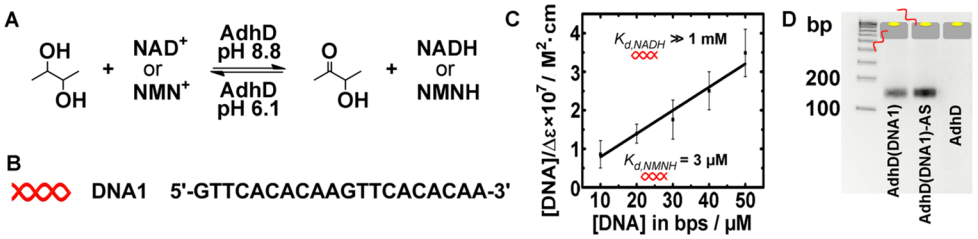

E

	AdhD-Ordered Bi-Bi Kinetics	k_{cat} (s^{-1})	$K_{D,cof}$ (μM)	$K_{M,cof}$ (μM)	$K_{M,diol}$ (mM)	K_i (μM)
NAD^+	AdhD	5.8±0.7	35±3	711±100	83±10	–
	AdhD(DNA1)	6.0±0.3	35±9	600±39	70±8	–
	AdhD(DNA1)-AS	6.0±0.4	34±5	623±65	62±7	–
NMN^+	AdhD	0.21±0.01	534±30	886±81	382±61	$\gg 10^4$
	AdhD(DNA1)	0.20±0.02	319±19 *	1046±367	406±22	12±0.7 *
	AdhD(DNA1)-AS	0.20±0.02	294±18	1038±115	406±33	10±0.8

Figure 4. Altering the kinetics of AdhD with the cofactor mimic NMN^+. (A) Oxidation and reduction reactions of AdhD. (B) Sequence of ssDNA1. (C) Binding assay of NMN(H) to dsDNA1. (D) Mobility shift assay of AdhD and AdhD conjugated with ssDNA1 by free lysines and near the active site (-AS). (E) Kinetics parameters of AdhD, AdhD(DNA1), and AdhD(DNA1)-AS ($n \geq 3$, * $p \leq 0.01$).

pairs.[22] Here, we demonstrated binding of the NAD(H) mimic NMN(H), and we have previously demonstrated micromolar affinity of phenolics to DNA.[17] Interactions between DNA and aniline are used to create templates for enzyme-mediated synthesis of polyaniline nanowires.[23] In addition, the negatively charged phosphate backbone of DNA provides electrostatic interactions between DNA and positively charged substrates, and DNA-aptamers provide engineerable small molecule binding.[24]

It follows from our hypothesis that a well-placed DNA on the surface of an enzyme whose substrate has favorable molecular interactions with the DNA will lead to increased effective molarity of the substrate and a change in kinetics. We recognize that the enhancements across examples were mild, including a 2.6-fold decrease in $K_{M,APP}$ for TMB, a 2-fold decrease in K_I for 4-NBH, and a 1.8-fold decrease for $K_{D,NMN}$, but the resulting functional effects are meaningful. The strategy improved HRP catalysis from an already efficient 1.4×10^6 M^{-1} s^{-1} to 3.5×10^6 M^{-1} s^{-1}. By comparison, point mutations to superoxide dismutase that increase electrostatic guidance of substrates to the active site enhance catalysis by 3-fold, and disruption of this guidance decreases catalysis by ~2-fold.[3] Our strategy was also able to affect already strong HRP inhibition by 4-NHB, decreasing a nanomolar K_I by 2-fold. With respect to cofactor binding to AdhD, the introduction of intermolecular interactions between NMN^+ and conjugated DNA enhanced NMN^+ binding leading to a 4.7-fold decrease in catalysis due to pronounced cofactor inhibition.

The enzyme engineering strategy presented here aims to control the chemical conditions in close proximity to the enzyme and active site through the introduction of molecular interactions between the substrates, inhibitors, cofactors, and conjugated DNA. A similar strategy has also been realized by graphing charged polymers to the surface of an enzyme[25] and by immobilizing enzymes on nanoparticles with controlled surface charge.[26] The model system in these cases was the protease chymotrypsin and selective engineering of the charge conditions local to the enzyme resulted in enhanced substrate selectivity and enzyme efficiency. Combined, these works along with the studies presented here point to a general strategy of enzyme engineering that can be used independently to design enzyme nanostructures with enhanced catalysis or together with traditional strategies focused the active site engineering.

■ ASSOCIATED CONTENT

Supporting Information

The following file is available free of charge on the ACS Publications website at DOI: 10.1021/acscatal.5b00130.

Materials and methods. Predicted binding of substrates to DNA. Melting temperatures of single- and double-stranded DNA. Substrate−DNA binding assay spectra. Predicted binding poses of TMB to DNA. Shift assays of enzyme−DNA structures. UV−vis analysis of HRP-(DNA1/2). Crystal structure of HRP. Kinetics of HRP and modified HRP with ABTS and TMB. Kinetic analysis of HRP with DNA1 in solution. Electrostatic mapping of enzymes and substrates. Kinetics of AdhD-(DNA1)/AS (PDF)

■ AUTHOR INFORMATION

Corresponding Author

*E-mail: iwheeldon@engr.ucr.edu.

Notes

The authors declare no competing financial interest.

■ ACKNOWLEDGMENTS

We thank Shelley Minteer (University of Utah) for NMN^+ reduction catalysis. This study was supported by AFOSR (FA9550-13-1-0184) and NSF CAREER (MCB-1350401).

■ REFERENCES

(1) Getzoff, E. D.; Tainer, J. A.; Weiner, P. K.; Kollman, P. A.; Richardson, J. S.; Richardson, D. C. *Nature* **1983**, *306* (5940), 287−290.

(2) Perry, J. J. P.; Shin, D. S.; Getzoff, E. D.; Tainer, J. A. *Bba-Proteins Proteom* **2010**, *1804* (2), 245−262.

(3) Getzoff, E. D.; Cabelli, D. E.; Fisher, C. L.; Parge, H. E.; Viezzoli, M. S.; Banci, L.; Hallewell, R. A. *Nature* **1992**, *358* (6384), 347−351.

DOI: 10.1021/acscatal.5b00130
ACS Catal. 2015, 5, 2149−2153

(4) Choudhury, S. B.; Lee, J. W.; Davidson, G.; Yim, Y. I.; Bose, K.; Sharma, M. L.; Kang, S. O.; Cabelli, D. E.; Maroney, M. J. *Biochemistry-Us* **1999**, *38* (12), 3744−3752.
(5) Sussman, J. L.; Harel, M.; Frolow, F.; Oefner, C.; Goldman, A.; Toker, L.; Silman, I. *Science* **1991**, *253* (5022), 872−879.
(6) Nolte, H. J.; Rosenberry, T. L.; Neumann, E. *Biochemistry-Us* **1980**, *19* (16), 3705−3711.
(7) Silman, I.; Sussman, J. L. *Current opinion in pharmacology* **2005**, *5* (3), 293−302.
(8) Bommarius, A. S.; Paye, M. F. *Chem. Soc. Rev.* **2013**, *42* (15), 6534−6565.
(9) Bornscheuer, U. T.; Huisman, G. W.; Kazlauskas, R. J.; Lutz, S.; Moore, J. C.; Robins, K. *Nature* **2012**, *485* (7397), 185−194.
(10) Trudeau, D. L.; Smith, M. A.; Arnold, F. H. *Curr. Opin. Chem. Biol.* **2013**, *17* (6), 902−909.
(11) Reetz, M. T. *J. Am. Chem. Soc.* **2013**, *135* (34), 12480−12496.
(12) Campbell, E.; Meredith, M.; Minteer, S. D.; Banta, S. *Chem. Commun.* **2012**, *48* (13), 1898−1900.
(13) Rye, D. B.; Saper, C. B.; Wainer, B. H. *J. Histochem Cytochem* **1984**, *32* (11), 1145−1153.
(14) Aljofan, M.; Porotto, M.; Moscona, A.; Mungall, B. A. *J. Virol Methods* **2008**, *149* (1), 12−19.
(15) Josephy, P. D.; Eling, T.; Mason, R. P. *J. Biol. Chem.* **1982**, *257* (7), 3669−3675.
(16) Aitken, S. M.; Ouellet, M.; Percival, M. D.; English, A. M. *Biochem. J.* **2003**, *375*, 613−621.
(17) Lin, J.-L.; Wheeldon, I. *ACS Catal.* **2013**, *3* (4), 560−564.
(18) Morris, G. M.; Goodsell, D. S.; Halliday, R. S.; Huey, R.; Hart, W. E.; Belew, R. K.; Olson, A. J. *J. Comput. Chem.* **1998**, *19* (14), 1639−1662.
(19) Wheeldon, I. R.; Campbell, E.; Banta, S. *J. Mol. Biol.* **2009**, *392* (1), 129−142.
(20) Campbell, E.; Wheeldon, I. R.; Banta, S. *Biotechnol. Bioeng.* **2010**, *107* (5), 763−774.
(21) Segel, I. H. Wiley Classic Library ed.; Wiley-Interscience Publication: New York, 1993; p 957.
(22) Kellogg, G. E.; Scarsdale, J. N.; Fornari, F. A. *Nucleic Acids Res.* **1998**, *26* (20), 4721−4732.
(23) Ma, Y. F.; Zhang, J. M.; Zhang, G. J.; He, H. X. *J. Am. Chem. Soc.* **2004**, *126* (22), 7097−7101.
(24) Wilson, D. S.; Szostak, J. W. *Annu. Rev. Biochem.* **1999**, *68*, 611−647.
(25) Murata, H.; Cummings, C. S.; Koepsel, R. R.; Russell, A. J. *Biomacromolecules* **2014**, *15* (7), 2817−2823.
(26) You, C. C.; Agasti, S. S.; De, M.; Knapp, M. J.; Rotello, V. M. *J. Am. Chem. Soc.* **2006**, *128* (45), 14612−14618.

DOI: 10.1021/acscatal.5b00130
ACS Catal. 2015, 5, 2149−2153